On the flow of a stress power-law fluid in an orthogonal rheometer

On the Flow of a Stress Power-Law Fluid in an Orthogonal Rheometer

Lorenzo Fusi*, Benedetta Calusi, Angiolo Farina

Università degli Studi di Firenze, Dipartimento di Matematica e Informatica "Ulisse Dini", Viale Morgagni 67/A, 50134 Firenze, Italy.

Kumbakonam R. Rajagopal

Texas A&M University, Department of Mechanical Engineering, 301 Olsen Blvd, College Station, TX 77845, USA

Abstract

The orthogonal rheometer, an instrument developed by Maxwell and Chartoff [1] that has been used to measure the properties of non-Newtonian fluids, is essentially two parallel disks rotating about non-coincident axes with the same angular speed. By measuring the forces due to the flow of the fluid, and corroborating the constitutive relation with the same, one can determine the material moduli that characterize the fluid. In this paper, we discuss the flow of a novel constitutive relation that has been developed to describe the response of colloids. We find that pronounced boundary layers adjacent to the rotating plates can develop even at moderate Reynolds. These boundary layers are not necessarily restricted to inertial boundary layers. The flow patterns are also markedly different from those for the classical Navier-Stokes or power-law fluids.

Keywords: Stress power-law fluids, Constitutive relations for Colloids, Orthogonal rheometer, Boundary layers.

*Corresponding author
Email address: lorenzo.fusi@unifi.it (Lorenzo Fusi)

1. Introduction

Studies of flows between rotating plates have a long history, the details of which can be found in Rajagopal [2]. There have been numerous studies following the pioneering work of Von Karman [3] where axi-symmetric solutions for the flow due to two infinite parallel disks rotating over a common axis were found. Our interests here are in flows due to two parallel disks rotating about non-coincident axes that do not have axial symmetry. Even the case of flows with axial symmetry for a Navier-Stokes fluid provides very interesting possibilities for non-unique solution (see Batchelor [4], Stewartson [5] Holodniok and Kubicek [6], and the numerous references in Rajagopal [2]).

In an ingenious study, Berker [7] found solutions that are not axially symmetric due to flows between infinite parallel plates rotating about a common axis. Such a situation would be obtained when one also has a pressure gradient imposed on the flow. The form of solutions that Berker assumed are also suitable for analyzing the solutions that are relevant to the flow between disks rotating about non-coincident axis. The flows sought by Berker for the flow between two plates rotating with the same angular speed in the same direction belong to the class of pseudo-planar flows that he studied earlier in detail (see Berker [8]). Pseudo-planar flows are essentially plane flows, but the structure of the planar flows varies in the different planes along the normal to the planes and there is no flow in the direction normal to the planes. Abbot and Walters [9] obtained an exact solution to the problem of a Navier-Stokes fluid flowing between infinite parallel plates rotating about non-coincident axis with different angular speeds, but this solution was anticipated earlier by Berker and had gone unnoticed (Berker [7]). Flows occurring between parallel plates due to the plates rotating with the same angular speed, but about different axes, is in essence an instrument that is used to characterize the material moduli of non-Newtonian fluids. The device, which has finite parallel plates rotating with the same angular speed about non-coincident axes, known as the orthogonal rheometer, was devised by Maxwell and Chartoff [1].

The flows occurring in such a device can be approximated as motions with constant principal stretch history (see Noll [10] for a definition of motions with constant principal stretch history), and the flows of all Simple Fluids (see Noll [11]) occurring between parallel plates rotating about non-coincident axes simplify to a very simple structure (see Rajagopal [12]). Measuring the shear and normal forces acting on the plates, one can determine the material moduli that characterize the non-Newtonian fluid that is in the device. There have been many studies concerning flows in an orthogonal rheometer for a variety of non-Newtonian fluids (see Blyler and Kurtz [13], Bird and Harris [14], R. R. Huilgol [15], Kearsley [16], Goddard [17], Goldstein and Schowalter [18], Kaloni and Siddiqui [19], Rajagopal [20], Rajagopal et al. [21], Bower et al. [22], Rajagopal and Wineman [23]). All the studies mentioned above are special sub-classes of simple fluids.

Recently, Rajagopal [24] (see also Rajagopal [25]) generalized the class of Simple Fluids to include a much larger class of fluids wherein the constitutive relation is given in terms of an implicit functional that depends on both the history of the stress and the history of the relative deformation gradient (see also Prusa and Rajagopal [26]). A special sub-class of these fluids are generalized stress-power law fluids introduced by Malek et al. [27]. These fluids exhibit markedly distinct flow behavior than classical power-law fluids. Srinivasan and Karra [28] studied the flows of stress power-law fluids flowing in an orthogonal rheometer and they found the development of boundary layers at sufficiently low Reynolds numbers if the power-law exponent was in a particular range. Le Roux and Rajagopal [29] modified the stress power-law model, and the modification allows one to fit data for flows of colloids very well (see data for colloidal solutions in Boltenhagen et al. [30], and corroboration of the constitutive relation due to Le Roux and Rajagopal [29] by Perlacova and Prusa [31]). Le Roux and Rajagopal [29] studied simple shearing flows of the constitutive relation that they had proposed, between two parallel plates. Janecka et al. [32] studied numerically the cylindrical Couette flow of the fluid in between two cylinders rotating about a common axis and also the flow in a narrowing channel. Recently, Fusi et al. [33] studied the flow of such a fluid past a porous plate subject to suction, and they also studied the stability of such flows.

Here, we are interested in studying the flow of a fluid described by the constitutive relation developed by Le Roux and Rajagopal [29] in an orthogonal rheometer. In addition to the boundary layer that manifests itself at high Reynolds numbers, we find that at even low Reynolds number, if the exponent n is appropriate, pronounced boundary layers may develop. The effects of the viscosity are restricted to a narrow region adjacent to the two rotating plates and in a large central core region, the fluid rotates as though it is a rigid body.

In Section 2 we introduce the constitutive relation that we are interested in studying, and in the following Section we derive the governing equations for the flow in an orthogonal rheometer and render them non-dimensional. In Section 4, for the sake of comparison and to highlight the markedly distinct characteristics of the flow of our fluid of interest, we document the exact solutions for the Navier-Stokes fluid in an orthogonal rheometer. Section 5 is devoted to a discussion of the numerical procedure that is used to solve the governing equations and this is followed in the subsequent Section where a different scaling is used to render the equations dimensionless. In the final Section we discuss the results of the numerical solution.

2. The mathematical model

We consider a class of incompressible fluids whose Cauchy stress is related to the fluid motion through[1] $\mathbf{T}^* = -p^*\mathbf{I} + \mathbf{S}^*$, where

$$\mathbf{D}^* = \alpha^* \left[\left(1 + \beta^* \mathrm{tr}{\mathbf{S}^*}^2 \right)^n + \gamma \right] \mathbf{S}^*. \tag{1}$$

In the above equation, $\mathbf{D}^*$ is the symmetric part of the velocity gradient, $-p^*\mathbf{I}$ is the indeterminate part of the stress due to the constraint of incompressibility, n is the stress power-law index, and α^* and β^* are positive constant. The term

[1]Throughout the paper the starred variables represent dimensional quantities.

multiplying the deviatoric stress $\mathbf{S}^*$ is the generalized fluidity that depends on the stress. Fluids described by such a constitutive relation were introduced in Máletk et al. [27]. The main feature of these fluids is that symmetric part of the velocity gradient is given as a function of the stress and not the stress in terms of the symmetric part of the velocity gradient. The class of fluids introduced in Máletk et al. [27] are special sub-classes of constitutive relations wherein the stress and the symmetric part of the velocity gradient are related implicitly (see Rajagopal [29] for a discussion of general algebraic implicit equations). The principal characteristic of (1) is that the stress power-law model can allow for a relation wherein the shear rate is a non-monotone function of the shear stress and the shear stress is therefore not a function of the shear rate. This possibility is a crucial feature of the response of some colloids, see Boltenhagen et al. [30], Hu et al. [34]. When $n < -1/2$ and

$$\gamma < 2 \left[\frac{|2n+1|}{2(1-n)} \right]^{1-n}, \tag{2}$$

the shear-rate vs shear-stress relation is non monotone (S shaped), in the case of Simple Shear flow, see Le Roux et al. [29].

3. Governing equations

We study the flow in an orthogonal rheometer as the one depicted in Fig. 1. We consider a set of cylindrical coordinates (r^*, θ, z^*), the z^*-axis being placed symmetrically between the two axes of rotation (see again Fig. 1). The device consists of two parallel disks rotating about two non-coincident axes placed at distance $2a^*$ apart. In particular, the upper plate, at $z^* = 2h^*$, rotates about an axis through P, and the bottom plate, at $z^* = 0$, rotates about an axis through Q. The two parallel plates rotate in the same direction with the same angular velocity Ω^*, which is constant in time. The velocity field $\mathbf{v}^* = v_r^* \mathbf{e}_r + v_\theta^* \mathbf{e}_\theta + v_z^* \mathbf{e}_z$ satisfies the following boundary conditions:

$$\mathbf{v}^* = \Big[\Omega^* a^* \cos\theta, \Omega^* \left(r^* - a^* \sin\theta \right), 0 \Big], \qquad \text{on} \quad z^* = 2h^*, \tag{3}$$

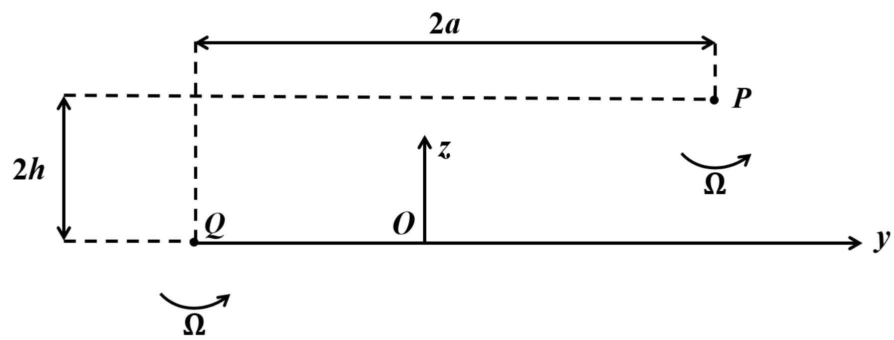

Figure 1: Schematic of an orthogonal rheometer. The origin of the coordinate system is O.

$$\mathbf{v}^* = \Big[-\Omega^* a^* \cos\theta, \Omega^* \left(r^* + a^* \sin\theta\right), 0\Big], \qquad \text{on} \quad z^* = 0. \tag{4}$$

The equations governing the flow of the fluid are

$$\begin{cases} \rho^* \dfrac{D\mathbf{v}^*}{Dt^*} = -\nabla p^* + \nabla\cdot\mathbf{S}^* - \rho^* g^* \mathbf{e}_z, \\ \\ \nabla\cdot\mathbf{v}^* = 0, \end{cases} \tag{5}$$

where D/Dt^* denotes the material derivative, g^* the gravity acceleration and the second of the equations is a consequence of the requirement that the flows is isochoric. By using the non-dimensionalization

$$\begin{aligned} &z^* = h^*\left(z+1\right), \quad r^* = a^* r, \quad t^* = \frac{1}{\Omega^*} t, \quad v_r^* = \Omega^* a^* v_r, \\ &v_\theta^* = \Omega^* a^* v_\theta, \quad v_z^* = \Omega^* h^* v_z, \quad \mathbf{S}^* = S_c^* \mathbf{S}, \quad p^* = S_c^* p, \end{aligned} \tag{6}$$

with S_c^* being the characteristic stress still to be selected, system (5) and the boundary conditions (3), (4), become

$$\begin{cases} \left(\dfrac{\rho^* {\Omega^*}^2}{S_c^* {a^*}^{-2}}\right) \dfrac{Dv_r}{Dt} = -\dfrac{\partial p}{\partial r} + \left[\dfrac{1}{r}\dfrac{\partial \left(r S_{rr}\right)}{\partial r} + \dfrac{1}{r}\dfrac{\partial S_{r\theta}}{\partial \theta} - \dfrac{S_{\theta\theta}}{r} + \left(\dfrac{a^*}{h^*}\right)\dfrac{\partial S_{rz}}{\partial z}\right], \\ \\ \left(\dfrac{\rho^* {\Omega^*}^2}{S_c^* {a^*}^{-2}}\right) \dfrac{Dv_\theta}{Dt} = -\dfrac{\partial p}{\partial \theta}\dfrac{1}{r} + \left(\dfrac{S_c^*}{a^*}\right)\left[\dfrac{1}{r^2}\dfrac{\partial \left(r^2 S_{r\theta}\right)}{\partial r} + \dfrac{1}{r}\dfrac{\partial S_{\theta\theta}}{\partial \theta} + \left(\dfrac{a^*}{h^*}\right)\dfrac{\partial S_{\theta z}}{\partial z}\right], \\ \\ \left(\dfrac{\rho^* {\Omega^*}^2}{S_c^* {h^*}^{-2}}\right) \dfrac{Dv_z}{Dt} = -\left(\dfrac{\rho^* g^*}{S_c {h^*}^{-1}}\right) - \dfrac{\partial p}{\partial z} + \\ \\ + \left(\dfrac{h^*}{a^*}\right)\left[\dfrac{1}{r}\dfrac{\partial \left(r S_{rz}\right)}{\partial r} + \dfrac{1}{r}\dfrac{\partial S_{\theta z}}{\partial \theta} + \left(\dfrac{a^*}{h^*}\right)\dfrac{\partial S_{zz}}{\partial z}\right], \\ \\ \dfrac{1}{r}\dfrac{\partial \left(r v_r\right)}{\partial r} + \dfrac{1}{r}\dfrac{\partial v_\theta}{\partial \theta} + \dfrac{\partial v_z}{\partial z} = 0, \end{cases} \tag{7}$$

and

$$\begin{cases} \mathbf{v} = (\cos\theta, r - \sin\theta, 0), & \text{on} \qquad z = 1, \\ \\ \mathbf{v} = (-\cos\theta, r + \sin\theta, 0), & \text{on} \qquad z = -1, \end{cases} \tag{8}$$

respectively. We introduce the ratio between the distance separating the disks and their axes through

$$\xi = \left(\frac{h^*}{a^*}\right), \tag{9}$$

and set

$$S_c^* =: S^* = \left(\frac{\Omega^*}{2\alpha^* \xi}\right), \qquad \frac{\beta}{2} = \frac{\beta^* {\Omega^*}^2}{4{\alpha^*}^2 \xi^2}, \tag{10}$$

so that

$$\mathbf{D} = \left[\left(1 + \frac{\beta}{2}\mathrm{tr}\mathbf{S}^2\right)^n + \gamma\right]\mathbf{S}. \tag{11}$$

We seek velocity field of the form $\mathbf{v} = v_r \mathbf{e}_r + v_\theta \mathbf{e}_\theta$, where

$$v_r = A(z)\cos\theta + B(z)\sin\theta, \quad v_\theta = r + B(z)\cos\theta - A(z)\sin\theta, \tag{12}$$

which automatically fulfills the requirement that the flows is isochoric $(7)_4$. Because of the particular form of the velocity field, the deviatoric stress $\mathbf{S}$ is chosen to be

$$\mathbf{S} = X(z,\theta)\Big[\mathbf{e}_r \otimes \mathbf{e}_z + \mathbf{e}_z \otimes \mathbf{e}_r\Big] + Y(z,\theta)\Big[\mathbf{e}_\theta \otimes \mathbf{e}_z + \mathbf{e}_z \otimes \mathbf{e}_\theta\Big]. \tag{13}$$

Therefore, equations $(7)_{1-3}$ can be rewritten as

$$\begin{cases} \mathsf{Re}\left[-r-(B\cos\theta - A\sin\theta)\right] = -\dfrac{\partial p}{\partial r} + \dfrac{1}{\xi}\dfrac{\partial X}{\partial z}, \\ \\ \mathsf{Re}\left(A\cos\theta + B\sin\theta\right) = -\dfrac{1}{r}\dfrac{\partial p}{\partial \theta} + \dfrac{1}{\xi}\dfrac{\partial Y}{\partial z}, \\ \\ 0 = -\phi - \dfrac{\partial p}{\partial z}, \end{cases} \tag{14}$$

where

$$\mathsf{Re} = 2\alpha^*\rho^*\Omega^*{a^*}^2\xi, \tag{15}$$

is the Reynolds number and

$$\phi = \left(\frac{2\alpha^*\rho^*g^*a^*\xi}{\Omega^*}\right),$$

is the non-dimensional pressure gradient in the z direction. The boundary conditions (8) acquire the forms

$$\begin{cases} A(-1) = -1, \quad A(1) = 1, \\ \\ B(-1) = 0, \qquad B(1) = 0. \end{cases} \tag{16}$$

Recalling that $\mathrm{tr}\mathbf{S}^2 = 2\left(X^2+Y^2\right)$ we find

$$\begin{aligned} D_{rz} &= A'\cos\theta + B'\sin\theta = \left\{\left[1+\beta\left(X^2+Y^2\right)\right]^n + \gamma\right\} X, \\ D_{\theta z} &= B'\cos\theta - A'\sin\theta = \left\{\left[1+\beta\left(X^2+Y^2\right)\right]^n + \gamma\right\} Y, \end{aligned} \tag{17}$$

where $(\cdot)'$ denotes the derivative w.r.t. z. As a consequence, we see that X^2+Y^2 depends only on z since

$${A'}^2 + {B'}^2 = \left\{\left[1+\beta\left(X^2+Y^2\right)\right]^n + \gamma\right\}^2\left(X^2+Y^2\right).$$

Focussing on equation $(14)_3$, we obtain

$$p = -\phi z + \mathcal{F}(r, \theta). \tag{18}$$

We then consider equations $(14)_1$ and $(14)_2$ which we differentiate w.r.t. z, obtaining

$$\begin{cases} -\mathsf{Re}\,(B' \cos\theta - A' \sin\theta) = \dfrac{1}{\xi} X'', \\ \\ \mathsf{Re}\,(A' \cos\theta + B' \sin\theta) = \dfrac{1}{\xi} Y'', \end{cases} \tag{19}$$

which, on exploiting (17), gives rise to

$$\begin{cases} X'' = -\overline{\mathsf{Re}} \left\{ \left[1 + \beta \left(X^2 + Y^2\right)\right]^n + \gamma \right\} Y, \\ \\ Y'' = \overline{\mathsf{Re}} \left\{ \left[1 + \beta \left(X^2 + Y^2\right)\right]^n + \gamma \right\} X, \end{cases} \tag{20}$$

where

$$\overline{\mathsf{Re}} = \xi \mathsf{Re},$$

where ξ is given by (9). Recalling (18), it is straightforward to see that equations $(14)_1$ and $(14)_2$ entail

$$p = -\phi z + \mathsf{Re} \frac{r^2}{2} + r \mathcal{N}(\theta) + p_0,$$

where p_0 is a constant and $\mathcal{N}$ is a function depending (possibly) on θ. However, assuming the absence of flows due to a prescribed horizontal pressure gradient, and thus $\mathcal{N} = 0$, we obtain

$$p = \mathsf{Re} \frac{r^2}{2} - \phi z + p_0. \tag{21}$$

By substituting (21) into $(14)_{1,2}$ and using (16), we obtain the following boundary conditions

$$\begin{cases} X'(-1, \theta) = -\overline{\mathsf{Re}} \sin\theta, \quad X'(1, \theta) = \overline{\mathsf{Re}} \sin\theta, \\ \\ Y'(-1, \theta) = -\overline{\mathsf{Re}} \cos\theta, \quad Y'(1, \theta) = \overline{\mathsf{Re}} \cos\theta. \end{cases} \tag{22}$$

The solution to system (20) coupled with boundary conditions (22), provides $A(z)$ and $B(z)$ through (19), namely

$$\begin{cases} A\left(z\right) = \dfrac{X'}{\mathsf{Re}} \sin\theta + \dfrac{Y'}{\mathsf{Re}} \cos\theta, \\ \\ B\left(z\right) = \dfrac{Y'}{\mathsf{Re}} \sin\theta - \dfrac{X'}{\mathsf{Re}} \cos\theta, \end{cases} \tag{23}$$

and, as a consequence, the velocity field through (12). Notice that necessarily $X(z,\theta)$, $Y(z,\theta)$ are such that the dependence on θ on the right hand side of (23) is cancelled. We finally observe that in cartesian coordinates the velocity field is

$$v_x = A(z) - y, \qquad v_y = B(z) + x, \qquad v_z = 0,$$

so that $\mathcal{C} = \Big[-B(z), A(z), z \Big]$ with $z \in [-1, 1]$ represents the locus of the centers of rotation.

Remark 1. *When the constitutive law is non monotonic there exist multiple shear stresses corresponding to a unique shear rate. Hence, in principle, one could find (numerically) more than one solution to the problem* (20)*. When solving the problem numerically, we have observed that the iterative procedure (based on Newton's methods) converges always to the same solution (independently of the initial guess), which is the one corresponding to the first "monotonically increasing branch" of the constitutive law, i.e. the one with the smallest shear stress. A possible explanation of this fact is that the steady solutions with larger shear rate are unstable and hence the iterative numerical method cannot converge to these solutions. Another possible explanation is the following: we notice that problem* (20) *is a nonlinear BVP in* $X(z)$ *and* $Y(z)$ *with boundary data involving the first derivatives of* $X(z)$ *and* $Y(z)$*. For this type of problem we do not have a standard well-posedness theorem as in the case of Cauchy problem, even if the numerical method seems to indicate uniqueness of a solution. Problem* (20) *is a consequence of the assumption that the velocity field has the form* $\mathbf{v} = (A(z) - y, B(z) + x, 0)$*. Assuming other forms of the velocity field (e.g. with non-vanishing z component) could, in principle, lead to other* *solutions. So it could be possible that our BVP has only a unique solutions for which the z component is vanishing, while the other solutions are such that they have a non-vanishing z component. It is our intention to study this issue in the next future.*

4. Solution for flows of the Navier-Stokes fluid

For the sake of completeness and since we will be using the solution to the flow of a Navier-Stokes fluid to validate the numerical scheme, we shall provide a short discussion of the exact solution of the problem in the case of the Newtonian fluid.

In this case $n = 0$, $\gamma = 0$ or $\beta = 0$ and $\gamma = 0$. Following Abbott et al. [9], we may integrate the system (20), (22) and get

$$X = \sin\zeta\Big[C_1(\theta)e^{\zeta} + C_2(\theta)e^{-\zeta}\Big] + \cos\zeta\Big[C_1(\theta)e^{-\zeta} - C_2(\theta)e^{\zeta}\Big], \tag{24}$$

where

$$\zeta = \frac{z\eta}{\sqrt{2}}, \qquad \eta^2 = \overline{Re}.$$

The functions $C_j(\theta)$ are given by

$$C_1 = -\mathcal{K}\Big[\cos\theta(\mathcal{J} + \mathcal{I}) + \sin\theta(\mathcal{J} - \mathcal{I})],$$

$$C_2 = \mathcal{K}\Big[\cos\theta(\mathcal{I} - \mathcal{J}) + \sin\theta(\mathcal{I} + \mathcal{J})],$$

where

$$\mathcal{K} = \frac{\eta\sqrt{2}e^{\frac{\eta\sqrt{2}}{2}}}{8\Big[\cos\big(\frac{\eta\sqrt{2}}{2}\big)\Big]^2 e^{\eta\sqrt{2}} - 4e^{\eta\sqrt{2}} - 2e^{2\eta\sqrt{2}} - 2},$$

$$\mathcal{J} = \Big[e^{\eta\sqrt{2}} - 1\Big]\cos\big(\frac{\eta\sqrt{2}}{2}\big), \qquad \mathcal{I} = \Big[e^{\eta\sqrt{2}} + 1\Big]\sin\big(\frac{\eta\sqrt{2}}{2}\big).$$

The function Y is obtained from $Y = -\overline{Re}^{-1}X''$. Substituting the functions X,

Y into (23), we get

$$
\begin{aligned}
A(z) = -\frac{\mathrm{e}^{-\frac{\eta\sqrt{2}(-1+z)}{2}}}{d}\Big[&\cos\left(\tfrac{\eta\sqrt{2}}{2}\right)\left(\mathrm{e}^{\eta\sqrt{2}(z+1)}-\mathrm{e}^{\eta\sqrt{2}}-\mathrm{e}^{\eta z\sqrt{2}}+1\right)\cos\left(\tfrac{\eta z\sqrt{2}}{2}\right)+\\
&+\sin\left(\tfrac{\eta z\sqrt{2}}{2}\right)\sin\left(\tfrac{\eta\sqrt{2}}{2}\right)\left(\mathrm{e}^{\eta\sqrt{2}(z+1)}+\mathrm{e}^{\eta\sqrt{2}}+\mathrm{e}^{\eta z\sqrt{2}}+1\right)\Big],\\
B(z) = -\frac{\mathrm{e}^{-\frac{\eta\sqrt{2}(-1+z)}{2}}}{d}\Big[&-\sin\left(\tfrac{\eta\sqrt{2}}{2}\right)\left(\mathrm{e}^{\eta\sqrt{2}(z+1)}-\mathrm{e}^{\eta\sqrt{2}}+\mathrm{e}^{\eta z\sqrt{2}}-1\right)\cos\left(\tfrac{\eta z\sqrt{2}}{2}\right)+\\
&+\cos\left(\tfrac{\eta\sqrt{2}}{2}\right)\sin\left(\tfrac{\eta z\sqrt{2}}{2}\right)\left(\mathrm{e}^{\eta\sqrt{2}(z+1)}+\mathrm{e}^{\eta\sqrt{2}}-\mathrm{e}^{\eta z\sqrt{2}}-1\right)\Big],\\
d = 4\,\left(\cos\left(1/2\,\eta\sqrt{2}\right)\right)^2&\mathrm{e}^{\eta\sqrt{2}}-\mathrm{e}^{2\,\eta\sqrt{2}}-2\,\mathrm{e}^{\eta\sqrt{2}}-1.
\end{aligned}
\tag{25}
$$

The above functions $A(z)$, $B(z)$ provides the locus center of rotation in the Newtonian case. The Navier-Stokes solution can be used to validate the numerical scheme that is presented in the next Section.

5. Numerics

The nonlinear differential system (20), (22) is discretized by a spectral collocation method based on Chebyshev polynomials, Canuto et al. [35]. The system is solved via Newton's method imposing an initial guess. More specifically, we discretize X and Y on the Gauss-Lobatto points

$$z_j = \cos\left(\frac{j\pi}{N}\right), \qquad j = 0, ..., N$$

and we solve

$$\mathbf{W}_{m+1} = \mathbf{W}_m - \Big[\mathbf{J}^{-1}(\mathbf{W}_m)\Big]\mathbf{F}(\mathbf{W}_m), \tag{26}$$

where

$$\mathbf{W} = \begin{bmatrix} \mathbf{X} \\ \\ \mathbf{Y} \end{bmatrix} = \Big[X_0, ..., X_N, Y_0, ..., Y_N\Big]^T,$$

$$\mathbf{F}(\mathbf{W}) = \begin{bmatrix} \mathbf{D}_N^2\mathbf{X} + \mathrm{diag}\Big(\mathbf{f}(\mathbf{X})\Big)\mathbf{Y} \\ \\ \mathbf{D}_N^2\mathbf{Y} - \mathrm{diag}\Big(\mathbf{f}(\mathbf{X})\Big)\mathbf{X} \end{bmatrix},$$

where $\mathbf{f}(\mathbf{X})$ is the vector such that

$$f_i = \overline{\mathsf{Re}}\Big\{\big[1+\beta(X_i^2+Y_i^2)\big]^n + \gamma\Big\}, \qquad i = 0, ..., N.$$

where $\mathbf{D}_N$ is the Chebyshev differentiation matrix defined in Trefethen [36] and where $\mathbf{J}$ is the Jacobian of $\mathbf{F}$. We solve (26) starting with an initial guess $\mathbf{W}_0$ and we stop the iterative procedure when

$$\|\mathbf{W}_{m+1} - \mathbf{W}_m\| < 10^{-12}.$$

6. A different scaling

The scaling of the stress $(10)_1$ does not take into account the shear-thinning (or shear-thickening) behavior of the fluid. Indeed, the expression for S^* given in $(10)_1$ does not contain the exponent n and, as a consequence, the Reynolds numbers Re and $\overline{\mathsf{Re}}$ are independent of n. We can define a different Reynolds number in which the effect of the exponent n is included. To do this we rewrite the constitutive equation (1) in the following way

$$\mathbf{D}\left(\frac{\Omega^*}{2\xi}\right) = \underbrace{\alpha^*{\beta^*}^n {S_c^*}^{2n}}_{\alpha_g^*} S_c^*\left[\left(\frac{1}{\beta^* {S_c^*}^2} + \mathrm{tr}\,\mathbf{S}^2\right)^n + \frac{\gamma}{(\beta^* {S_c^*}^2)^n}\right]\mathbf{S}, \tag{27}$$

where α_g^* has the dimension of the inverse of a viscosity. We select the characteristic stress as

$$S_c^* =: \Sigma^* = \left[\frac{\Omega^*}{2\xi\alpha^*{\beta^*}^n}\right]^{\frac{1}{2n+1}}, \tag{28}$$

so that the constitutive equation (27) becomes

$$\mathbf{D} = \left[\left(\frac{1}{\beta^*{\Sigma^*}^2} + \mathrm{tr}\,\mathbf{S}^2\right)^n + \frac{\gamma}{(\beta^*{\Sigma^*}^2)^n}\right]\mathbf{S}.$$

Notice that (28) can be rewritten as

$$\Sigma^* = \left[\left(\frac{\Omega^*}{2\xi\alpha^*}\right)^2\beta^*\right]^{\frac{1}{2(2n+1)}} {\beta^*}^{-\frac{1}{2}} = \left[{S^*}^2\beta^*\right]^{\frac{1}{2(2n+1)}} {\beta^*}^{-\frac{1}{2}}, \tag{29}$$

which represents the link between the characteristic stresses S^* and Σ^*. The scaling (29) is acceptable for any value of n except $n = -1/2$. Recalling (15) we define the Reynolds with respect to α_g^*, namely

$$\mathsf{R}_\Sigma = \Big(2\rho^*\Omega^*{a^*}^2\xi\,\underbrace{\alpha^*{\beta^*}^n{\Sigma^*}^{2n}}_{\alpha_g^*}\Big) = \mathsf{Re}\Big(\beta^*{\Sigma^*}^2\Big)^n. \tag{30}$$

We notice that

$$\beta^*{\Sigma^*}^2 = \left[\beta^*\left(\frac{\Omega^*}{2\xi\alpha^*}\right)^2\right]^{\frac{1}{2n+1}} = \left(\frac{\beta}{2}\right)^{\frac{1}{2n+1}}, \tag{31}$$

so that

$$\mathsf{R}_\Sigma = \mathsf{Re}\left(\frac{\beta}{2}\right)^{\frac{n}{2n+1}}, \tag{32}$$

providing the relation between the two Reynolds numbers R_Σ and Re. Moreover, we can easily show that

$$S^* = \Sigma^*\left(\frac{\beta}{2}\right)^{-\frac{n}{2n+1}}.$$

Therefore, if we denote with σ_{ij} the non dimensional stress relative to the scaling Σ^* and S_{ij} the non dimensional stress relative to S^* we can write

$$S_{ij} = \frac{S_{ij}^*}{S^*} = \frac{S_{ij}^*}{\Sigma^*}\left(\frac{\beta}{2}\right)^{\frac{n}{2n+1}} = \sigma_{ij}\left(\frac{\beta}{2}\right)^{\frac{n}{2n+1}}.$$

In conclusion, we can state that the conversion factor between the two scalings is

$$\left(\frac{\beta}{2}\right)^{\frac{n}{2n+1}}.$$

From (32) we see that

$$\begin{aligned} &\beta > 2 \quad \Longrightarrow \quad \lim_{n\to-\left(\frac{1}{2}\right)^+}\mathsf{R}_\Sigma = 0^+, \qquad \lim_{n\to-\left(\frac{1}{2}\right)^-}\mathsf{R}_\Sigma = \infty, \\ &\beta < 2 \quad \Longrightarrow \quad \lim_{n\to-\left(\frac{1}{2}\right)^+}\mathsf{R}_\Sigma = \infty, \qquad \lim_{n\to-\left(\frac{1}{2}\right)^-}\mathsf{R}_\Sigma = 0^+. \end{aligned} \tag{33}$$

so that, depending on the constant β and on the value of n, the Reynolds number R_Σ can become very large or very small as n approaches the value $-1/2$.

7. Results

In this Section we shall present some numerical results to investigate the behavior of the stress components and to pinpoint the locus of the centers of rotation. We shall consider both scalings and we shall investigate the behavior of the solution and the possible formation of boundary layers. As a first example we consider a flow with a moderate Reynolds number, i.e. $\overline{Re} = 20$, with $\gamma = 0.2$ and $\beta = 0.2$. In Fig. 2 we plot the 3D curve representing the locus of the centers of rotation for different values of n, including one for which the constitutive relation is non monotone. In this first example the scaling is the one presented in Section 3. In Figs 3, 4 we plot the stresses S_{xy}, S_{yz}.

When considering the scaling of Section 6, i.e. the one in which the Reynolds number depends also on n, it is evident that we may observe the development of boundary layers even in the case of moderate Reynolds number. In the case of Navier-Stokes fluid this behavior is not observed, as boundary layers form only at high values of the Reynolds number. This is a peculiarity also observed in Srinivasan et al. [28].

In the Figs 5-6 we plot the projections of the center of rotation on the planes $y = 0$ and $x = 0$ for various n, with the scaling introduced in Section 6. We use $\mathsf{R}_\Sigma = 50$, $\beta = \gamma = 0.2$. In Figs 7-8 we show the stresses S_{xz} and S_{yz} for the same ranges of n. In Figs 9, 10 we plot a close up of the stresses for $n = -0.3, 0, 0.5$. As expected the formation of the boundary layers occurs for values of n close to the critical values $n = -1/2$. In the Figs 11-14 we plot again the projections of the centers of rotation and the stresses S_{xz}, S_{yz} with $\mathsf{R}_\Sigma = 5$, $\beta = 2.5$ and $\gamma = 0.2$. In Figs 16, 10 we plot a close up of the stresses for the cases $n = -0.6$, $n = 0$, $n = 0.5$. Once again we observe that boundary layers develop for n close to $-1/2$.

It is evident that the value of the exponent n plays a crucial role in the development of the boundary layers. In particular, we notice that the value $n = -1/2$, which marks the transition between the monotone and non monotone constitutive law for suitable values of the constant γ, marks also the transition

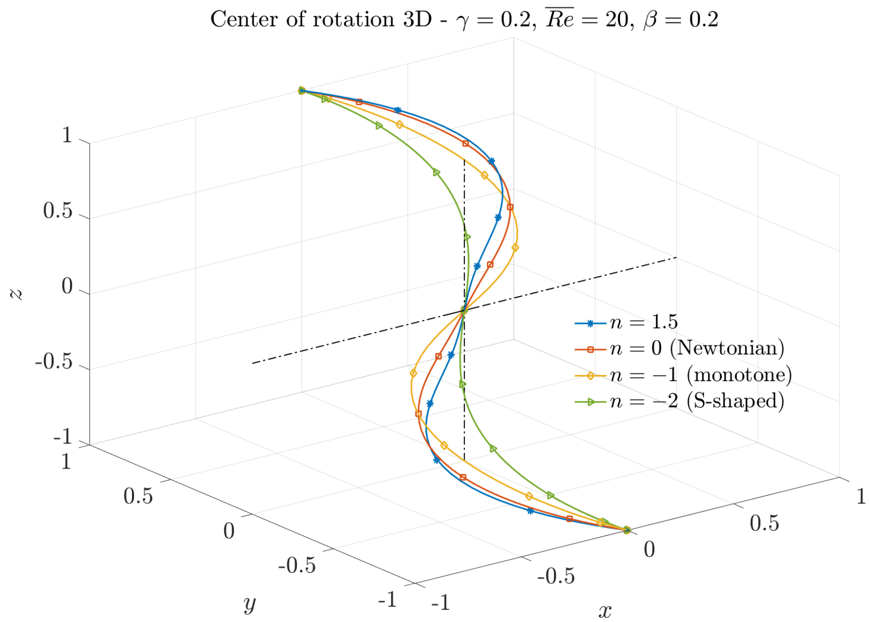

Figure 2: Locus of the centers of rotation.

from a "true" pseudo-planar flow to one in which the velocity field varies only in a thin boundary layer adjacent to the rotating disks.

Acknowledgement

The present work has been performed under the auspices of the Italian National Group for Mathematical Physics (GNFM-Indam).

References

[1] B. Maxwell, R. Chartoff, Studies of a polymer melt in an orthogonal rheometer, Transactions of the Society of Rheology 9 (1) (1965) 41–52.

[2] K. Rajagopal, Flow of viscoelastic fluids between rotating disks, Theoretical and Computational Fluid Dynamics 3 (4) (1992) 185–206.

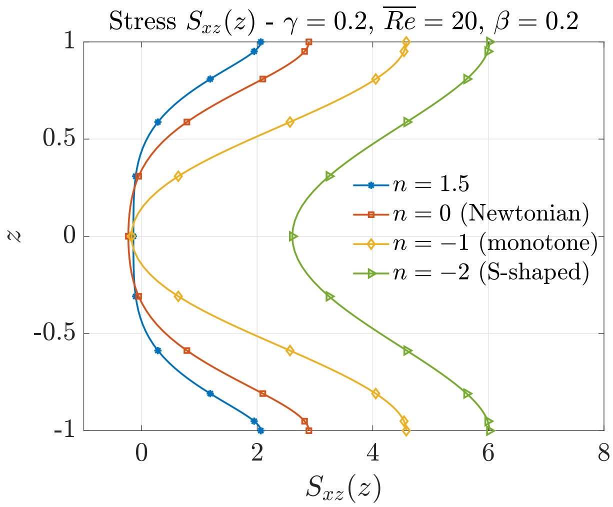

Figure 3: Stress $S_{xz}(z)$.

[3] T. Von Kármán, Uber laminare und turbulente reibung, Z. Angew. Math. Mech. 1 (1921) 233–252.

[4] G. K. Batchelor, Note on a class of solutions of the navier-stokes equations representing steady rotationally-symmetric flow, The Quarterly Journal of Mechanics and Applied Mathematics 4 (1) (1951) 29–41.

[5] K. Stewartson, On the flow between two rotating coaxial disks, Mathematical Proceedings of the Cambridge Philosophical Society 49 (2) (1953) 333–341.

[6] M. Holodniok, M. Kubicek, V. Hlavácek, Computation of the flow between two rotating coaxial disks, Journal of Fluid Mechanics 81 (1977) 689–699.

[7] R. Berker, A new solution of the navier-stokes equation for the motion of a fluid contained between two parallel plates rotating about the same axis, Archiv of Mechanics, Archiwum Mechaniki Stosowanej 31 (2) (1979) 265–280.

[8] R. Berker, Intégration des équations du mouvement d'un fluide visqueux incompressible, Handbuch der physik 3 (1963) 1–384.

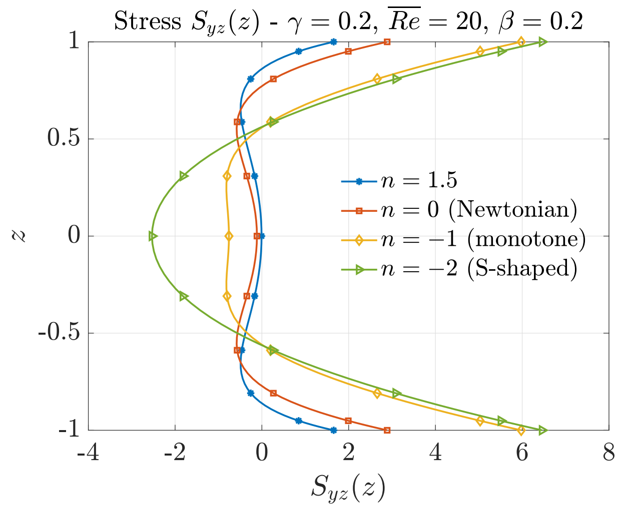

Figure 4: Stress $S_{yz}(z)$.

[9] T. Abbott, K. Walters, Rheometrical flow systems part 2. theory for the orthogonal rheometer, including an exact solution of the navier-stokes equations, Journal of Fluid Mechanics 40 (1) (1970) 205–213.

[10] W. Noll, A mathematical theory of the mechanical behavior of continuous media, in: The Foundations of Mechanics and Thermodynamics, Springer, 1974, pp. 1–30.

[11] W. Noll, Motions with constant stretch history, Archive for Rational Mechanics and Analysis 11 (1) (1962) 97–105.

[12] K. Rajagopal, On the flow of a simple fluid in an orthogonal rheometer, Archive for Rational Mechanics and Analysis 79 (1) (1982) 39–47.

[13] L. Blyler Jr, S. Kurtz, Analysis of the maxwell orthogonal rheometer, Journal of Applied Polymer Science 11 (1) (1967) 127–131.

[14] R. B. Bird, E. K. Harris Jr, Analysis of steady state shearing and stress relaxation in the maxwell orthogonal rheometer, AIChE Journal 14 (5) (1968) 758–761.

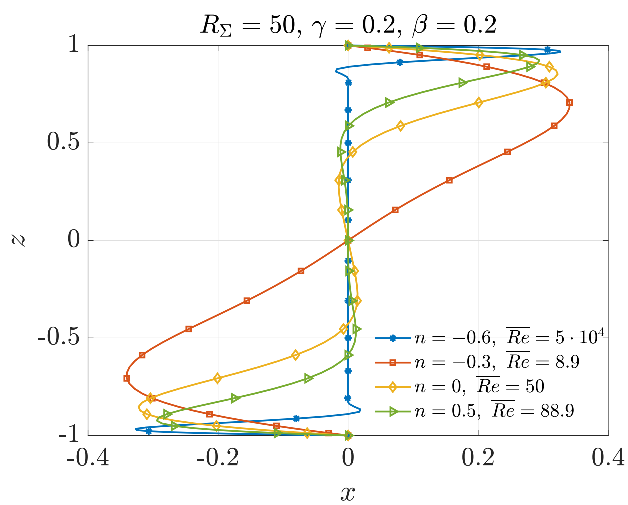

Figure 5: Projection of the locus of centers of rotation on the plane $y = 0$ for various n: $\mathsf{R}_\Sigma = 50$, $\beta = 0.2$, $\gamma = 0.2$.

[15] R. Huilgol, On the properties of the motion with constant stretch history occurring in the maxwell rheometer, Transactions of the Society of Rheology 13 (4) (1969) 513–526.

[16] E. A. Kearsley, On the flow induced by a maxwell-chartoff rheometer, Journal of Research of the National Bureau of Standards: Engineering and instrumentation 72 (1968) 23.

[17] J. Goddard, The dynamics of simple fluids in steady circular shear, Quarterly of Applied Mathematics 41 (1) (1983) 107–118.

[18] C. Goldstein, W. Schowalter, Further studies of fluid nonlinearity: The orthogonal rheometer and the oscillating sphere, Transactions of the Society of Rheology 19 (1) (1975) 1–19.

[19] P. Kaloni, A. Siddiqui, A note on the flow of a viscoelastic fluid between eccentric disks, Journal of non-newtonian fluid mechanics 26 (1) (1987) 125–133.

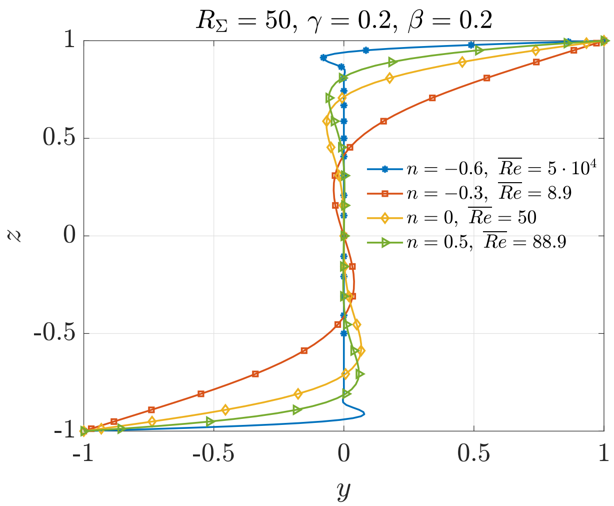

Figure 6: Projection of the locus of centers of rotation on the plane $x = 0$ for various n: $\mathsf{R}_\Sigma = 50$, $\beta = 0.2$, $\gamma = 0.2$.

[20] K. Rajagopal, The flow of a second order fluid between rotating parallel plates, Journal of Non-Newtonian Fluid Mechanics 9 (1-2) (1981) 185–190.

[21] K. Rajagopal, M. Renardy, Y. Renardy, A. Wineman, Flow of viscoelastic fluids between plates rotating about distinct axes, Rheologica acta 25 (5) (1986) 459–467.

[22] M. Bower, A. S. Wineman, K. R. Rajagopal, Flow of k-bkz fluids between parallel plates rotating about distinct axes: shear thinning and inertial effects, Journal of non-newtonian fluid mechanics 22 (3) (1987) 289–307.

[23] K. Rajagopal, A. Wineman, Flow of a bkz fluid in an orthogonal rheometer, Journal of Rheology 27 (5) (1983) 509–516.

[24] K. R. Rajagopal, On implicit constitutive theories, Applications of Mathematics 48 (4) (2003) 279–319.

[25] K. Rajagopal, On implicit constitutive theories for fluids, Journal of Fluid Mechanics 550 (2006) 243–249.

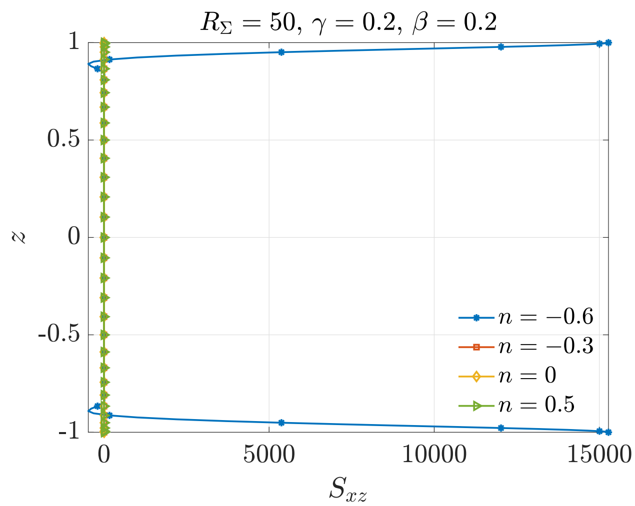

Figure 7: Stress S_{xz} for various n: $\mathsf{R}_\Sigma = 50$, $\beta = 0.2$, $\gamma = 0.2$.

[26] V. Prusa, K. Rajagopal, On implicit constitutive relations for materials with fading memory, Journal of Non-Newtonian Fluid Mechanics 181 (2012) 22–29.

[27] J. Málek, V. Prusa, K. Rajagopal, Generalizations of the navier–stokes fluid from a new perspective, International Journal of Engineering Science 48 (12) (2010) 1907–1924.

[28] S. Srinivasan, S. Karra, Flow of "stress power-law" fluids between parallel rotating discs with distinct axes, International Journal of Non-Linear Mechanics 74 (2015) 73–83.

[29] C. Le Roux, K. R. Rajagopal, Shear flows of a new class of power-law fluids, Applications of Mathematics 58 (2) (2013) 153–177.

[30] P. Boltenhagen, Y. Hu, E. Matthys, D. Pine, Observation of bulk phase separation and coexistence in a sheared micellar solution, Physical review letters 79 (12) (1997) 2359.

[31] T. Perlácová, V. Prusa, et al., Tensorial implicit constitutive relations

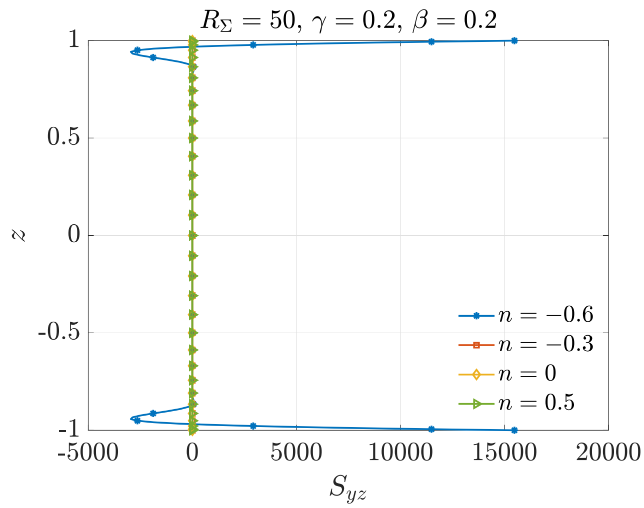

Figure 8: Stress S_{yz} for various n: $\mathsf{R}_\Sigma = 50$, $\beta = 0.2$, $\gamma = 0.2$.

in mechanics of incompressible non-newtonian fluids, Journal of Non-Newtonian Fluid Mechanics 216 (2015) 13–21.

[32] A. Janevka, J. Malek, V. Prusa, G. Tierra, Numerical scheme for simulation of transient flows of non-newtonian fluids characterised by a non-monotone relation between the symmetric part of the velocity gradient and the cauchy stress tensor, Acta Mechanica 230 (2019) 729–747.

[33] L. Fusi, G. Saccomandi, K. R. Rajagopal, L. Vergori, Flow past a porous plate of non-newtonian fluids with implicit shear stress shear rate relationships, European Journal of Mechanics - B/Fluids 92 (2022) 166–173.

[34] Y. Hu, P. Boltenhagen, D. Pine, Shear thickening in low-concentration solutions of wormlike micelles. i. direct visualization of transient behavior and phase transitions, Journal of Rheology 42 (5) (1998) 1185–1208.

[35] C. Canuto, M. Y. Hussaini, A. Quarteroni, A. Thomas Jr, et al., Spectral methods in fluid dynamics, Springer Science & Business Media, 2012.

[36] L. N. Trefethen, Spectral methods in MATLAB, SIAM, 2000.

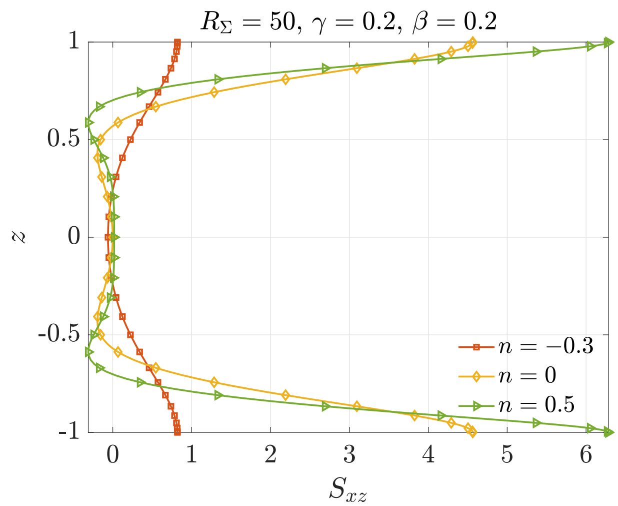

Figure 9: Stress S_{xz} for $n = -0.3, 0, 0.5$: $\mathsf{R}_\Sigma = 50$, $\beta = 0.2$, $\gamma = 0.2$.

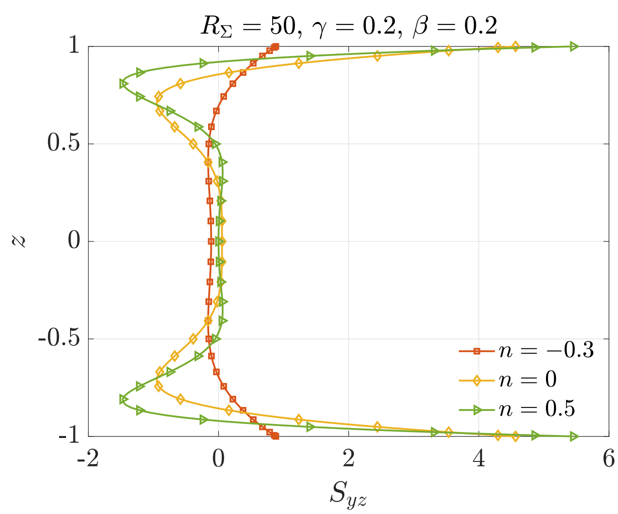

Figure 10: Stress S_{yz} for $n = -0.3, 0, 0.5$: $\mathsf{R}_\Sigma = 50$, $\beta = 0.2$, $\gamma = 0.2$.

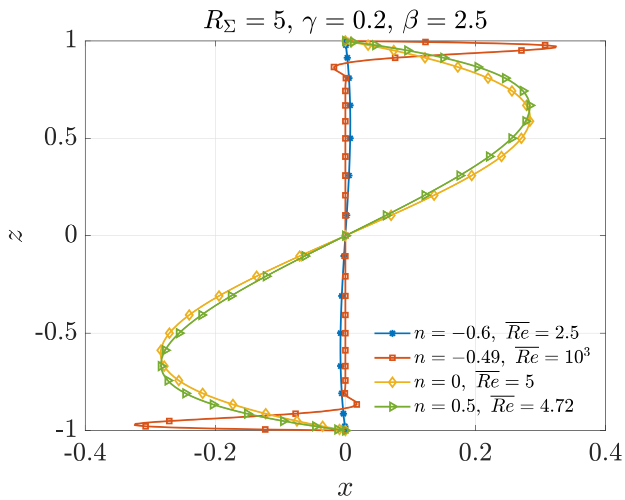

Figure 11: Projection of the locus of centers of rotation on the plane $y = 0$ for various n: $\mathsf{R}_\Sigma = 5$, $\beta = 2.5$, $\gamma = 0.2$.

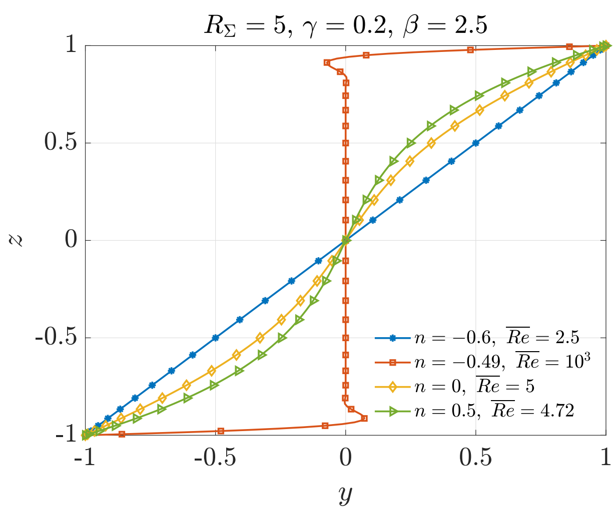

Figure 12: Projection of the locus of centers of rotation on the plane $x = 0$ for various n: $\mathsf{R}_\Sigma = 5$, $\beta = 2.5$, $\gamma = 0.2$.

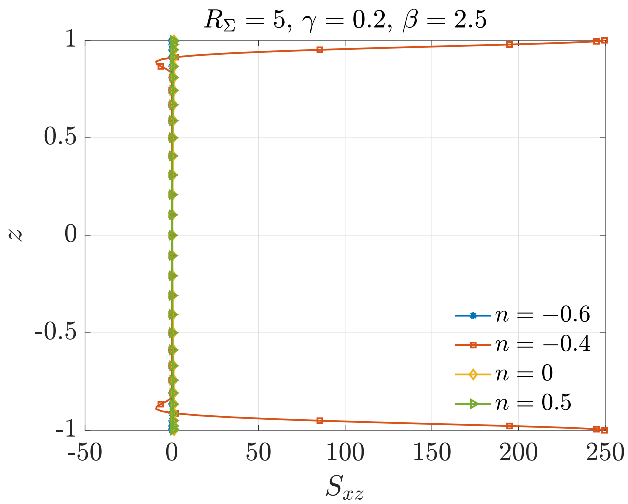

Figure 13: Stress S_{xz} for various n: $\mathsf{R}_\Sigma = 5$, $\beta = 2.5$, $\gamma = 0.2$.

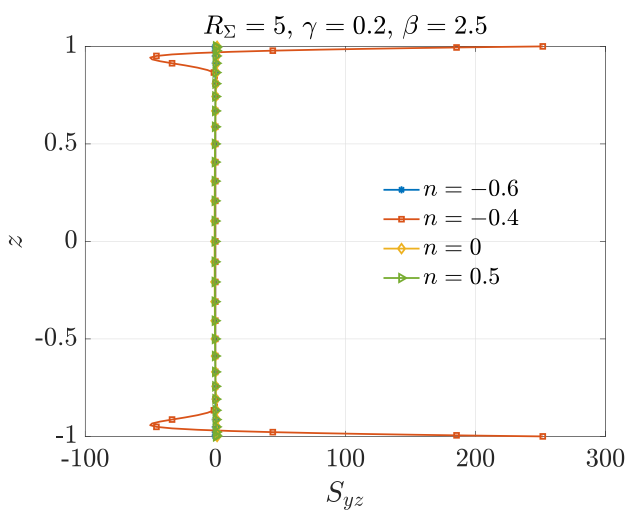

Figure 14: Stress S_{yz} for various n: $\mathsf{R}_\Sigma = 5$, $\beta = 2.5$, $\gamma = 0.2$.

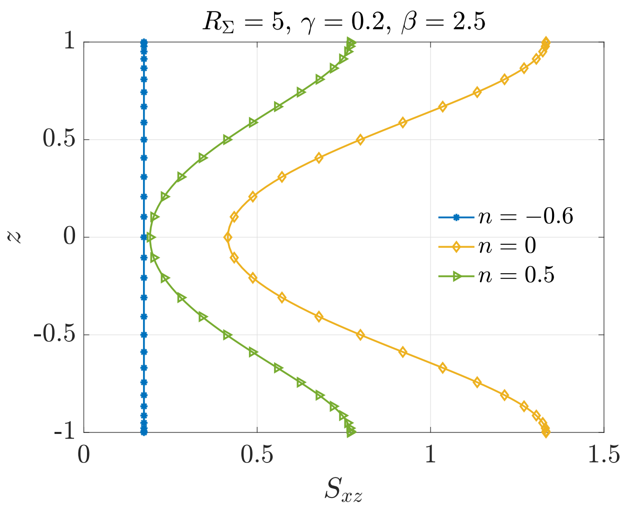

Figure 15: Stress S_{xz} for $n = -0.6, 0, 0.5$: $\mathsf{R}_\Sigma = 5$, $\beta = 2.5$, $\gamma = 0.2$.

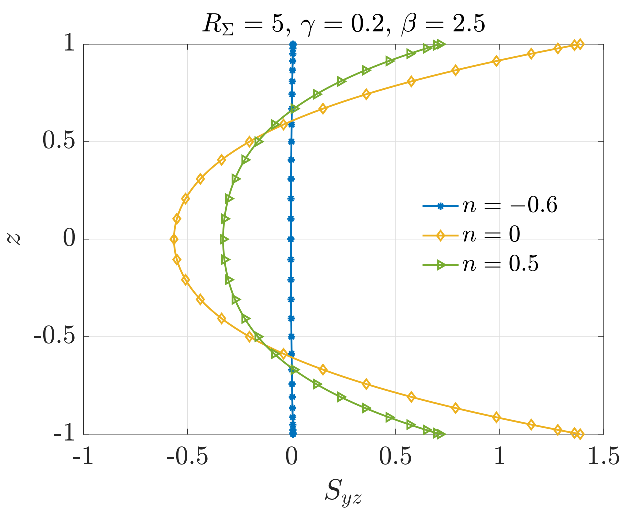

Figure 16: Stress S_{yz} for $n = -0.6, 0, 0.5$: $\mathsf{R}_\Sigma = 5$, $\beta = 2.5$, $\gamma = 0.2$.